

# Electronic Structure and Magnetic Exchange Coupling in Ferromagnetic Full Heusler Alloys

Yasemin Kurtulus, Richard Dronskowski

*Institut für Anorganische Chemie,  
Rheinisch-Westfälische Technische Hochschule,  
52056 Aachen, Germany*

German Samolyuk, Vladimir P. Antropov

*Ames Laboratory,  
Ames, IA, 50011, USA*

(Dated: May 1, 2019)

## Abstract

Density-functional studies of the electronic structures and exchange interaction parameters have been performed for a series of ferromagnetic full Heusler alloys of general formula  $\text{Co}_2\text{MnZ}$  ( $Z = \text{Ga}, \text{Si}, \text{Ge}, \text{Sn}$ ),  $\text{Rh}_2\text{MnZ}$  ( $Z = \text{Ge}, \text{Sn}, \text{Pb}$ ),  $\text{Ni}_2\text{MnSn}$ ,  $\text{Cu}_2\text{MnSn}$  and  $\text{Pd}_2\text{MnSn}$ , and the connection between the electronic spectra and the magnetic interactions have been studied. Different mechanisms contributing to the exchange coupling are revealed. The band dependence of the exchange parameters, their dependence on volume and valence electron concentration have been thoroughly analyzed within the Green function technique.

PACS numbers:

Keywords: Heusler alloys, ferromagnetism, electronic structure, Curie temperature, exchange parameter

## I. INTRODUCTION

The evolving field of spin-electronics has triggered an increasing interest in materials with full spin polarization at the Fermi level. Many of these systems have been predicted by means of electronic band-structure calculations [1, 2], and some of them are in use already as elements in multi-layered magneto-electronic devices such as magnetic tunnel junctions [3, 4] and also as giant magneto-resistance spin valves [5]. Promising device candidates are characterized by a strong spin polarization, by high Curie temperatures and by a large band gap, too. Among the most popular groups of materials is the extraordinarily large family of magnetic Heusler alloys [6] which is traditionally considered to be an ideal local-moment system [7, 8, 9]. This implies that their exchange couplings can be described by a Heisenberg Hamiltonian which allows the investigation of the temperature properties of the magnetic systems within a very simple concept. It therefore seems that the problem of calculating the exchange interaction parameters with the help of reliable electronic structure methods must have a very high priority in this field.

Nonetheless, despite a thorough theoretical understanding of the electronic structures of many full Heusler alloys (see, for example, Refs. [9, 10, 11, 12, 13, 14, 15]), only very few publications are dedicated to the discussions of magnetic exchange interactions in these systems. Noda and Ishikawa [16] have extracted the exchange parameters from the spin-wave spectrum using a model-like Heisenberg fit. On the theoretical side, Kübler, Williams and Sommers focused on the calculated total-energy differences between the ferromagnetic (FM) and different antiferromagnetic (AFM) states [9]. The parameters of the Heisenberg Hamiltonian were then fitted to reproduce the course of the calculated energies but such technique usually allows to extract only the parameters of the first and second neighbors, and the interactions between Mn and all other atoms are neglected for reasons of simplicity.

In this contribution, we derive the magnetic exchange parameters of a number of Heusler alloys from first principles and then analyze the magnetic coupling dependence on electronic structure variations induced by atomic substitutions or volume variations. The paper is organized as follows: In the next section II we describe the crystal structure under investigation and the computational method chosen. Section III is devoted to the parameter-free derivation of exchange parameters by theoretical approaches within density-functional theory. Section IV contains our results for the electronic structures and the magnetic interaction

parameters of the  $\text{Co}_2\text{MnZ}$ ,  $\text{Rh}_2\text{MnZ}$  and  $\text{X}_2\text{MnSn}$  families of alloys. Finally, we summarize our results in section V.

## II. CRYSTAL STRUCTURE AND COMPUTATIONAL DETAILS

The Heusler alloys represent a class of ternary intermetallic compounds of general formula  $\text{X}_2\text{YZ}$  in which X is a transition metal, Z is a metal of main groups III–V, and Y is a magnetically active transition metal such as manganese. The Heusler alloys adopt ordered  $\text{L2}_1$  structures, given in Fig. 1, which may be understood as being the result of four interpenetrating face-centered cubic (fcc) lattices. According to the  $\text{L2}_1$  structure jargon, the X atoms occupy the A and C sites, the Y atoms are on the B sites and the Z atoms are found on the D sites. Thus, sites A, B, C and D correspond to the positions  $(0,0,0)$ ,  $(\frac{1}{4},\frac{1}{4},\frac{1}{4})$ ,  $(\frac{1}{2},\frac{1}{2},\frac{1}{2})$  and  $(\frac{3}{4},\frac{3}{4},\frac{3}{4})$  within the fcc supercell [17].

The uniqueness of the Heusler alloys is due to the fact that they exhibit cooperative magnetic phenomena — especially ferromagnetism — in the desired temperature range although no constituent of their archetype,  $\text{Cu}_2\text{MnAl}$ , exhibits such properties in the elemental state. Even simpler than  $\text{Cu}_2\text{MnAl}$  is the phase  $\text{MnAl}$  which also displays strong ferromagnetic behavior and is of technological interest because of an enhanced magnetic anisotropy. The tetragonal  $\text{MnAl}$  ground state results from two subsequent (electronic and structural) distortions away from a cubic structure [18]. The group of cubic Heusler alloys considered in this paper, however, all contain Mn atoms as the Y atoms, and all phases exhibit ferromagnetic order. Their lattice parameters, magnetic saturation moments and also experimental Curie temperatures are shown in Tab. I.

For the band-structure calculation we used the TB-LMTO-ASA method [19, 20], including combined corrections, and took the experimental values of the lattice parameters. The local-density approximation (LDA) according to the Vosko–Wilk–Nusair exchange-correlation functional was used [21]. The summation over the entire Brillouin zone (BZ) was performed with a total of 195  $\mathbf{k}$  points in the irreducible part of the BZ.

### III. THE CALCULATION OF EXCHANGE-INTERACTIONS PARAMETERS IN DENSITY-FUNCTIONAL THEORY

The exchange coupling parameter  $J_{ij}$  between two centers  $i$  and  $j$  being part of a magnetic material is usually defined in the following standard procedure of the so-called rigid spin approximation (RSA),

$$J_{ij} = \mathbf{m}_i \frac{\partial^2 E}{\partial \mathbf{m}_i \partial \mathbf{m}_j} \mathbf{m}_j = \mathbf{m}_i [\chi]_{ij}^{-1} \mathbf{m}_j, \quad (1)$$

where  $E$  is the total energy of the system,  $\mathbf{m}_i$  is the magnetic moment on site  $i$ , and  $\chi_{ij}$  is a magnetic susceptibility.

In the above eq. 1, the entry  $\chi$  can be considered the adiabatic (static) limit of the transversal part of the spin-dynamical susceptibility

$$\chi(\mathbf{q}, \omega) = \sum \frac{\varphi_\nu^\uparrow(\mathbf{k}) \varphi_{\nu'}^{*\uparrow}(\mathbf{k} + \mathbf{q}) \varphi_\nu^\downarrow(\mathbf{k}) \varphi_{\nu'}^{*\downarrow}(\mathbf{k} + \mathbf{q})}{\varepsilon_\nu^\uparrow(\mathbf{k}) - \varepsilon_{\nu'}^\downarrow(\mathbf{k} + \mathbf{q}) - \omega + i0}, \quad (2)$$

where  $\varphi_\nu^\uparrow(\mathbf{k})$  and  $\varepsilon_\nu^\uparrow(\mathbf{k})$  are eigenfunctions and eigenvalues of band structure problem, and the arrows designate the spin direction. The so-called static limit ( $\omega \rightarrow 0$ ) can be justified if

$$\varepsilon_\nu^\uparrow(\mathbf{k}) - \varepsilon_{\nu'}^\downarrow(\mathbf{k} + \mathbf{q}) = I m \gg \omega. \quad (3)$$

This condition (eq. 3) determines a whole range of spin-wave frequencies for which one may use the adiabatic approximation and proceed with the well-known Heisenberg model expression for the spin wave spectrum

$$\omega(\mathbf{q}) = m (J(\mathbf{q}) - J(0)) = m (\chi^{-1}(\mathbf{q}) - \chi^{-1}(0)). \quad (4)$$

Below we will estimate the validity of the above criterion (eq. 3) for several compounds studied in this paper. Whenever eq. 3 is satisfied in localized systems, however, eq. 1 can be further simplified and a long-wave approximation (LWA, with essentially similar smallness criteria as in the RSA) can be used to obtain the following expression,

$$J_{ij}^{\text{lw}} = \mathbf{m}_i [\chi]_{ij}^{-1} \mathbf{m}_j \approx \mathbf{m}_i \chi_i^{-1} \chi_{ij} \chi_j^{-1} \mathbf{m}_j \approx \mathbf{m}_i I_i \chi_{ij} I_j \mathbf{m}_j, \quad (5)$$

where  $\chi_i^{-1}$  is an on-site element of the inverted spin susceptibility. Due to this similarity one cannot use the static approximation (eq. 4 or any type of Heisenberg model) for large  $q$

vectors. The model will be correct for large  $q$  (or small distances in real space) only if *both* long-wave and adiabatic approximations are removed simultaneously.

The currently most practical expression for the exchange coupling is based on the Green function or multiple-scattering formalism. In this technique, an analogue of eq. 1 can be derived [22] which reads

$$\begin{aligned} J(\mathbf{q}) &= \frac{1}{N} \sum J_{ij} e^{i\mathbf{q}\mathbf{R}_{ij}} = \frac{1}{N} \sum \frac{1}{\pi} \int^{E_F} d\varepsilon \text{ImTr} \left\{ \Delta_i [T^\uparrow T^\downarrow]_{ij}^{-1} \Delta_j \right\} e^{i\mathbf{q}\mathbf{R}_{ij}} \\ &= \frac{1}{\pi} \int^{E_F} d\varepsilon \text{ImTr} \left\{ \Delta_i \left[ \int d\mathbf{k} T^\uparrow(\mathbf{k}) T^\downarrow(\mathbf{k} + \mathbf{q}) \right]^{-1} \Delta_i \right\}. \end{aligned} \quad (6)$$

where  $\Delta_i = T_{ii}^\uparrow - T_{ii}^\downarrow$  and

$$T_{ij}^\sigma = \frac{1}{\Omega_{BZ}} \int d\mathbf{k} T^\sigma(\mathbf{q}) e^{i\mathbf{q}\mathbf{R}_{ij}} = \frac{1}{\Omega_{BZ}} \int d\mathbf{k} (p^\sigma(\varepsilon) - S(\mathbf{q}))^{-1} e^{i\mathbf{q}\mathbf{R}_{ij}}. \quad (7)$$

Here,  $T^\sigma$  is a scattering path operator,  $p^\sigma(\varepsilon)$  is an atomic-potential scattering matrix and  $S$  is a matrix of structure constants. The corresponding long-wave limit was obtained in Ref. [23] and reads

$$J^{\text{lw}}(\mathbf{q}) = \frac{1}{\pi\Omega_{BZ}} \int \int^{E_F} d\mathbf{k} d\varepsilon \text{ImTr} \{ p_i T^\uparrow(\mathbf{k}) T^\downarrow((\mathbf{k} + \mathbf{q})) p_i \}, \quad (8)$$

where  $p = p^\uparrow - p^\downarrow$ . In real space, the zero-moment of exchange interactions can be calculated accordingly to the sum rule

$$J_i^{\text{lw}} = \sum_{j \neq i} J_{ij}^{\text{lw}} = \frac{1}{\pi} \int^{E_F} d\varepsilon \text{ImTr} [p_i \Delta_i + p_i T_i^\uparrow T_i^\downarrow p_i]. \quad (9)$$

The linearization of the multiple-scattering expression leads to the LMTO Green function formalism where in a two-center approximation the  $p^\sigma$  matrix can be replaced by its linearized analogue

$$p^\sigma(\varepsilon) = \frac{C^\sigma - \varepsilon}{\Delta^\sigma}, \quad (10)$$

with spin-dependent LMTO potential parameters, namely  $C^\sigma$  as the band center and  $\Delta^\sigma$  as its width. One can show [24] that whenever  $\Delta^\uparrow = \Delta^\downarrow$ , that is, equal bandwidth for different spin projections, the Fourier transform of eq. 8 can be written in the form of eq. 5. It is this limiting case which allows us to separate the susceptibility and magnetic moment amplitude contributions to the total exchange coupling. In the present paper, we will mostly use eq.

8 because of its simplicity, but the applicability of this approach will be checked and eq. 6 will be used if necessary.

Due to the presence of several magnetic atoms in a primitive cell, a multi-atomic expression for the Curie temperature has to be used. In the so-called mean field approximation (MFA), the Curie temperature  $T_C$  of the system with  $N$  nonequivalent magnetic atoms is calculated as a largest solution of the equation

$$\det[T_{nm} - T\delta_{nm}] = 0, \quad (11)$$

where  $n$  and  $m$  are the indices of the non-equivalent magnetic sublattices,  $T_{nm} = \frac{2}{3}J_{mn}^0$ , and  $J_{mn}^0$  is an effective interaction of an atom from sublattice  $n$  with all other atoms from the sublattice  $m$ . In our case with two non-equivalent magnetic atoms per cell, the expression for  $T_C$  is reduced to

$$T_C = \frac{1}{3}\{J_{\text{Mn-Mn}}^0 + J_{\text{X-X}}^0 + \sqrt{[J_{\text{Mn-Mn}}^0 - J_{\text{X-X}}^0]^2 + 4(J_{\text{Mn-X}}^0)^2}\}. \quad (12)$$

## IV. RESULTS AND DISCUSSION

### A. $\text{Co}_2\text{MnZ}$ ( $\text{Z} = \text{Ga, Si, Ge and Sn}$ ) compounds

To start with, we performed calculations of the electronic band structures of four Co-based Heusler alloys with the generic formula  $\text{Co}_2\text{MnZ}$  ( $\text{Z} = \text{Ga, Si, Ge and Sn}$ ). The results for the electronic spectra are in good agreement with existing calculations of the electronic structures of these compounds [9, 10, 11, 12, 13, 14]. To better analyze the density-of-states (DOS) curves presented later, we first schematically sketch the hybridizations [25] of the minority-spin orbitals between the Co and Mn atoms in  $\text{Co}_2\text{MnGa}$ , given in Fig. 2. It is justified to take the minority-spin orbitals because, due to the exchange hole, these lie higher in energy and are relatively diffuse such that they are much more involved in the chemical bonding [26]. Their larger diffuseness also leads to the finding that spin-polarized ground states show larger interatomic distances despite of having a lower total energy [27]. Compared to the case of  $\text{Co}_2\text{MnGe}$  [10], the Fermi energy ( $E_F$ ) in the  $\text{Z} = \text{Ga}$  case (see Fig. 2) is placed below the Co-Co  $t_{1u}$  and  $e_u$  orbitals. For  $\text{Co}_2\text{MnGe}$ , the  $t_{1u}$  orbital is filled with one extra electron.

Fig. 3 presents the spin-polarized DOS of  $\text{Co}_2\text{MnGa}$ , and the splittings between different symmetry states have been extracted at the zone center  $\Gamma$  for minority-spin states (see also

discussion in Ref. [10]). Note that this is an over-simplification because the symmetry labels are not strictly valid over the entire reciprocal space. As expected, the DOS around the Fermi level is heavily dominated by the  $3d$  states of the Mn and Co atoms, and the majority spin states are nearly fully occupied. The DOS curves for the minority spins exhibit two peaks above the Fermi level which are due to both Mn and Co  $3d$  contributions. The difference in the positions of these two peaks is directly determined by the difference in intra-atomic exchange splitting between Mn and Co. The broad structure in the lowest energy region between  $-0.8$  and  $-0.55$  Ry goes back to (magnetically inactive)  $4s$  and  $4p$  states of Ga, and they are well separated from the  $3d$  states positioned in an energy region between  $-0.45$  and  $0.3$  Ry. It is interesting to note that the Fermi level of  $\text{Co}_2\text{MnGa}$  is found at the DOS minimum of the minority states, but for  $Z = \text{Si}$  and  $\text{Ge}$  it is positioned exactly in a gap, that is, these two latter compounds exhibit 100% spin polarization. This gap has previously been reported by other authors and is formed due to the strong  $3d$ - $3d$  hybridization (orbital mixing) between the Co and Mn atoms [13, 14].

In such half-metallic compounds the total spin moment should ideally be an integer number (see discussion in Ref. [10]). Our results for the  $\text{Co}_2\text{MnZ}$  group, presented in Tab. I, are very close to that, and there is only a slight deviation from integer numbers reproducing so-called Slater–Pauling behavior: here, the total moment equals  $\mu_{\text{tot}} = N - 24$  where  $N$  is the total number of valence electrons in the unit cell. In accord with the DOS observation in Fig. 3, the  $Z$  ( $sp$ -type) atoms in  $\text{Co}_2\text{MnZ}$  have negligible moments. The minority-spin states of the Mn atoms are nearly empty (see also Fig. 3), and the values of the local Mn spin moments arrive at ca.  $3 \mu_{\text{B}}$ . The Co atoms do have significant spin moments, about  $0.7 \mu_{\text{B}}$  in  $\text{Co}_2\text{MnGa}$  and about  $1.0 \mu_{\text{B}}$  in the remaining compounds of this family. Clearly, and also most importantly, the exchange interactions between the Co and Mn atoms cannot be neglected *a priori*.

Accordingly, the calculated values of the partial contributions  $J_{mn}^0$  to the effective exchange parameter  $J_n^0$  are presented in Tab. II. As has been alluded to already, the interaction between Mn and Co atoms gives a *leading* contribution to the total effective coupling, thereby questioning the assumption used in earlier work [9] in that only Mn–Mn interactions were taken into consideration; in terms of  $3d$ - $3d$  orbital overlap, this leading contribution is not at all surprising. On the other side, the Co–Co interaction is negative ( $-0.36$  mRy) in  $\text{Co}_2\text{MnGa}$  and thereby demonstrates the tendency for AFM ordering in the Co sublattice.

This negative value, however, is compensated by the larger *positive* interaction between Co and Mn ( $J_{\text{Co-Mn}}^0 \approx 2 \times 2.9$  mRy) such that the *effective*  $J_0$  of Co remains large and positive. The Mn–Mn contribution to  $J_{\text{Mn}}^0$  is on the order of only 1 mRy, this is nearly five times smaller than the Co–Mn interaction.

For completeness, we mention that pure  $\alpha$ -Mn exhibits an AFM ordering at low temperature ( $J_0 < 0$ ), and the small positive exchange parameters by the nearest-neighbor Mn–Mn pairs in Mn-based Heusler compounds correspond to likewise positive and small second-neighbor pairs exchange parameters in pure  $\alpha$ -Mn. The theoretical values for the Curie temperatures  $T_C$  obtained by the MFA are also included in Tab. I. For  $\text{Co}_2\text{MnGa}$ ,  $T_C$  arrives at 635 K and underestimates the experimental value (694 K) by about 10%. Taking into account the fact that the MFA usually *overestimates* Curie temperatures, this must be considered an even larger disagreement with experiment.

To check the nature of this disagreement, we performed a calculation of  $J$  beyond the LWA using eq. 7. In Tab. I we also show the corresponding results obtained using this approach. Our calculations reveal that the effective coupling between the Mn atoms is practically unchanged so that the LWA is perfectly suitable for the description of this coupling. However, all other couplings are affected much more strongly by this approximation. For instance, the Co–Co interactions are modified nearly by a factor of two while Co–Mn interactions are increased by 25–35% overall. Correspondingly, the estimated critical temperatures of magnetic phase transition for this group of alloys are increased by 10–20 %, and they are larger than the experimentally observed quantities.

It follows from the results presented in Tab. II that the substitution of the main-group III element Ga by a main-group IV element such as Si, Ge or Sn leads to a significant increase of both  $J_{\text{Co-Mn}}^0$  and  $J_{\text{Mn-Mn}}^0$  values. Fortunately, the implications for the varying electronic structure introduced by such a substitution can be well described within the rigid-band approximation (RBA) (see Ref. [10, 14]). For illustration, Fig. 4 shows a comparison between the electronic structures of  $\text{Co}_2\text{MnGa}$  and  $\text{Co}_2\text{MnGe}$  in the energy region  $\pm 0.1$  Ry around the Fermi level. The zero energy in the lower DOS curve corresponds to the Fermi level of  $\text{Co}_2\text{MnGe}$  with 29 valence electrons; for  $\text{Co}_2\text{MnGa}$  with 28 valence electrons, the Fermi level is given by the solid vertical line in the upper DOS. Obviously, the DOS shapes for these two compounds are very similar to each other, a nice support for the reliability of the RBA. Thus, by simply changing the total number of valence electrons one may reproduce



the substitution of Ga by Ge fairly well, qualitatively.

Nonetheless, the total moment calculated from the electronic structure of  $\text{Co}_2\text{MnGa}$  only by extending the DOS to 29 valence electrons is just  $4.6 \mu_{\text{B}}$ , that is, 8% smaller than the numerical result ( $5 \mu_{\text{B}}$ ) for  $\text{Co}_2\text{MnGe}$ , and we will soon focus on this (small) discrepancy originating from differing interatomic distances. In the frame of the RBA, the significant increase in the exchange parameters (Tab. II) in going from  $\text{Co}_2\text{MnGa}$  to  $\text{Co}_2\text{MnGe}$  goes back to the shift of the Fermi energy (band filling in Ref. [28]) which corresponds to the one extra electron. This evolution of the effective parameters  $J_{\text{Mn}}^0 = J_{\text{Mn-Mn}}^0 + J_{\text{Mn-Co}}^0$  and also  $J_{\text{Co}}^0 = J_{\text{Co-Co}}^0 + J_{\text{Mn-Co}}^0/2$  as a function of the Fermi level is also included in Fig. 4. In fact, the  $J_0$  values of  $\text{Co}_2\text{MnGa}$  at the Fermi level of  $\text{Co}_2\text{MnGe}$  equal those of the real  $\text{Co}_2\text{MnGe}$  phase. Taking into consideration the usual MFA overestimation of the Curie temperatures, our calculation for  $\text{Co}_2\text{MnGe}$  gives an acceptable agreement (1115 K) with the experimental value of 905 K.

The dependence of the electronic structures and magnetic properties of the  $\text{Co}_2\text{MnZ}$  alloys on the chemical nature of the isoelectronic Z atom has already been discussed in Refs. [10, 11, 14, 15]. We will focus on the density of states (DOS) (see Fig. 5) of  $\text{Co}_2\text{MnZ}$  (Z = Si, Ge and Sn) which all display the same valence electron concentration. Not too surprisingly, the DOSs are similar to the preceding one of  $\text{Co}_2\text{MnGa}$ . However, all peaks below the Fermi level move to higher energies with increasing lattice parameters because of enlarging atomic radii. The latter results in a smaller overlap between the Mn  $3d$  and Co  $3d$  orbitals which, in turn, leads to a smaller dispersion of these bands [11], becoming more atomic-like. As a consequence, the DOS peaks come closer to each other and their amplitudes grow (Fig. 5).

Because the changes in peak positions with changing Z element is proportional to the change in the lattice parameter, the replacement of Si by Ge has smaller consequences than the replacement of Ge by Sn; in terms of radii (and chemical behavior), Si and Ge are more similar to each other. Thus, the movement in the DOS peaks is more distinct for  $\text{Co}_2\text{MnSn}$ . In agreement with the results of full-potential calculations [11], the Mn magnetic moment obtained in our TB-LMTO-ASA calculation slightly *increases* in the Si  $\rightarrow$  Ge  $\rightarrow$  Sn series. On the other hand, the Co magnetic moment is *lowered* so that the total magnetic moment is close to  $5 \mu_{\text{B}}$  in all three cases (see Tab. I). The increase of the Mn magnetic moment is consistent with the increase of the Mn-Mn contribution to the effective  $J_0$  (third column in Tab. II) in this series of compounds. The increase, however, is compensated by lower

values for the Co–Co and also Co–Mn interactions. Thus, the calculated  $T_C$ 's decrease along the line Si  $\rightarrow$  Ge  $\rightarrow$  Sn (see Tab. I), and this qualitative trend agrees with the tendency observed experimentally.

To fully demonstrate the volume dependence of the exchange interactions (and Curie temperatures, too), we also calculated the course of  $J_0$  in  $\text{Co}_2\text{MnSi}$  solely as a function of its volume. That is to say, the structure of  $\text{Co}_2\text{MnSi}$  was artificially expanded to lattice parameters that would better fit the compounds adopted by its higher homologues Ge and Sn; unfortunately, this is impossible to realize experimentally. Fig. 6 displays the values of the  $J_0$  parameters obtained from these calculations, and the purely volume-derived exchange parameters are in semi-quantitative agreement with those that go back to proper calculations of  $J_0$  for the real  $\text{Co}_2\text{MnGe}$  and  $\text{Co}_2\text{MnSn}$  systems with their correct lattice parameters. It is just too obvious that the behavior of the Curie temperature can therefore be explained by a simple volume effect when the Si atom is substituted by Ge or Sn.

A detailed comparison of Tabs. III and IV in terms of  $J_{ij}$  makes it clear that the interactions are relatively short ranged and do not exceed the, say, first four neighbors in each sublattice. The main exchange parameter,  $J_1$  of  $\text{Co}_1$ –Mn in Tab. III, corresponds to the nearest-neighbor Co–Mn interaction. This particular entry of the table alone already gives about 70% of the total contribution to  $J_0$  between Co and Mn atoms and is about ten times larger than the corresponding Co–Co and Mn–Mn interactions; a remarkable result but, as has been said before, not too surprising when considering the interatomic overlap. For comparison, Tab. III also contains the exchange parameters obtained in earlier work [9] where the authors calculated Mn–Mn exchange parameters from the total energy differences of the FM and AFM structures but by ignoring the Co–Mn interactions.

Naturally, their approach had to result in significantly larger Mn–Mn interactions in order to reproduce the FM/AFM energy differences because in such an approximation all interactions (Mn–Mn and Mn–Co) are effectively *mapped* into the Mn–Mn-type  $J_{ij}$ . Thus, one needs to compare an effective parameter for the Mn atom, namely  $J_{\text{Mn}}^0 = J_{\text{Mn–Mn}}^0 + J_{\text{Mn–Co}}^0$  from Tab. II with  $J_{\text{Mn}}^0 = 12 \times J_1 + 6 \times J_2$  from Ref. [9]. The obtained values are 10.9 mRy and 8.4 mRy correspondingly. This similarity between the results of the very different models suggests relatively localized magnetic character in this system.

## B. $\text{Rh}_2\text{MnZ}$ ( $Z = \text{Ge, Sn and Pb}$ ) compounds

Independent full-potential calculations of the electronic structure of this group have been published recently [10] and our results are in agreement with them. To ease the understanding of the new chemical system, we compare the densities-of-states of  $\text{Rh}_2\text{MnSn}$  with the preceding one of  $\text{Co}_2\text{MnSn}$ , and both are included in Fig. 7. Generally, the gap in the minority-spin states of the  $\text{Co}_2\text{MnZ}$  phases can also be observed for the  $\text{Rh}_2\text{MnZ}$  phases but this gap apparently becomes broader and the Fermi level is no longer found in the gap. Consequently, the total magnetic moment can no longer be an integer number for this group of intermetallic compounds, and the entries of Tab. I impressively support this statement.

Another important difference is given by the smaller width and also polarization of the rhodium  $3d$  states relative to those of cobalt. In chemical terms, this notable difference between the  $3d$  and  $4d$  (and also  $5d$ ) elements is easily explained by differences in spatial shielding, with interesting similarities to main-group chemistry [26]. In any case, the magnetic moment of the Rh atoms is only about half the size of those of the Co atoms, namely ca.  $0.45 \mu_{\text{B}}$  compared to ca.  $1 \mu_{\text{B}}$ .

In contrast to the Co-based system, the Mn moments in this group are larger by about  $0.6 \mu_{\text{B}}$ . Such a change has been explained [10] by a smaller hybridization between the Rh and Mn atoms than between the Co and Mn atoms. Alternatively, a chemical interpretation would focus on an effectively over-sized Mn atom because of the strongly widened lattice due to the large Rh atoms. Thus, the majority/minority spin splitting for Mn is strongly favored, and the intra-atomic exchange splitting will be mirrored by extraordinarily diffuse minority-spin orbitals for Mn. The same effect takes place in  $\text{FePd}_3$  where Fe acquires a very large moment because of being too spacious [26]. Unlike the results given in ref. [10], however, the total magnetic moments of our calculations do not monotonically increase in the row  $\text{Ge} \rightarrow \text{Sn} \rightarrow \text{Pb}$ , but this effect is probably related to the atomic spheres approximation used by us.

We will now analyze the results for the exchange coupling using eq. 5. The values of the exchange splittings  $m_i I_i$  for the Rh atoms are about three times smaller than for the Co atoms so that Rh–Rh and Rh–Mn exchange parameters are about ten and three times lower if compared to the Co–Co and Co–Mn pairs (see Tab. II) only because of this splitting renormalization. Such a simple explanation, however, is not applicable for the Mn–Mn

interactions where the corresponding susceptibility has also changed. In the Mn sublattice, the interactions are decreased in magnitude by about 1 mRy upon substitution of Co by Rh despite the increase of the Mn magnetic moments. Such a decrease for the Mn–Mn exchange parameters reflects a general AFM tendency for a nearly half-filled  $d$  band and an FM tendency for a nearly empty or filled  $d$  band; this has been discussed before [29]. As can be seen from Fig. 7, the manganese  $d$  states in the Rh-based compounds are nearly half filled while in Co-based compounds these Mn-centered states have been filled by approx. 0.6 electrons despite Co/Rh being isoelectronic.

When it comes to the volume dependence of the magnetic properties of the Rh-based compounds, we reiterate the course found for the  $\text{Co}_2\text{MnZ}$  ( $Z = \text{Ge}, \text{Sn}, \text{Pb}$ ) group (Fig. 5). One also expects a decrease of the Curie temperatures with increasing volume, and this is what the experimental  $T_C$  values reflect in the row  $\text{Ge} \rightarrow \text{Sn} \rightarrow \text{Pb}$  (see Tab. I). Unfortunately, this trend is somewhat obscured in the theoretical data. The calculated Curie temperatures in the LWA for  $\text{Rh}_2\text{MnSn}$  (435 K) and  $\text{Rh}_2\text{MnPb}$  (423 K) are not too far away from the experimental ones, 412 and 338 K respectively. For  $\text{Rh}_2\text{MnGe}$ , however, we underestimate  $T_C$  (410 K) compared to an experimental 450 K. The usage of eq. 6 leads to the significant modification of Rh–Rh coupling (factor of 2–3) and a 25–30% increase of the Rh–Mn coupling, *i.e.*, the MFA produces significantly larger numbers for  $T_C$ . However, all relative trends remain similar to the exchange coupling in the LWA.

The energy dependence of  $J$  in the  $\text{Rh}_2\text{MnZ}$  compounds with  $Z = \text{Ge}, \text{Sn}, \text{Pb}$ , depicted in Fig. 8, looks different from the one discussed before in the  $\text{Co}_2\text{MnZ}$  group. First, the amplitude of  $J(E)$  is smaller and, second, the maximum of the curve is a broad plateau. The last finding means that an increase of the electron concentration will *not* lead to a significant change for the exchange parameters. An alternative decrease of the electron concentration, however, leads to negative  $J$  values such that an FM state is no longer stable. For instance, the substitution of Ge by Al shifts the Fermi level down by 0.04 Ry (vertical line in Fig. 8) and leads to a significant decrease of  $J$ . This interpretation is supported by the experimental AFM ordering that was observed for  $\text{Rh}_2\text{MnAl}$  [30].

Closing this section, we'd like to mention that  $\text{Rh}_2\text{MnZ}$  compounds are traditionally discussed as systems with fully localized magnetic moments, in contrast to  $\text{Co}_2\text{MnZ}$ -type compounds where the Co magnetic moment can obviously not be neglected. The results for the effective  $J$  values in Tab. II and the pair-magnetic exchange values  $J_{ij}$  in Tab.

V clearly evidence that Rh–Mn interactions are even larger than Mn–Mn interactions. A similar behavior is known from Fe/Pd alloys where the Fe atom magnetically polarizes the  $4d$  metal upon strong Fe–Pd chemical bonding [26]. In the present case, the Rh–Mn exchange parameters are mostly determined by the first-neighbor  $J_1$  interaction. Mn–Mn interactions show a significantly longer range with the main contributions coming from large and positive  $J_1$ ,  $J_2$  and negative  $J_6$ .

### C. $\text{X}_2\text{MnSn}$ ( $\text{X} = \text{Ni}, \text{Cu}$ and $\text{Pd}$ ) compounds

In this section, we will analyze the change of the magnetic properties of the Heusler alloys upon atomic substitution by the X component, the non-Mn  $d$  metal. For the compounds with  $\text{X} = \text{Ni}, \text{Cu}$  and  $\text{Pd}$ , the electronic structures have been studied in Ref. [9, 10]. Similar to the preceding  $\text{Rh}_2\text{MnZ}$  group, the Fermi level is no longer in the minority-spin DOS gap and the total moment is not an integer number. The substitution of Co by Rh or Ni leads to a significant decrease of the  $d$ -metal polarization and, also, to a nearly complete filling of their minority-spin states. The magnetic moments of the X atoms is thereby reduced from  $1 \mu_B$  (Co) to ca.  $0.5 \mu_B$  (Rh) and, finally, to about  $0.2 \mu_B$  (Ni), given in Tab. I. This reduction is accompanied by an increase of the Mn magnetic moment only during the first substitution. The limiting case is given by the compounds with nonmagnetic Cu and Pd atoms.

Using the calculated magnetization values  $m_i$ , we can estimate the reduction of the  $J_{\text{X-X}}^0$  and  $J_{\text{X-Mn}}^0$  parameters (see discussion above). The obtained parameters give qualitative agreement with the directly calculated results, listed in Tab. II. However, this estimation can not reproduce the decrease of  $J_{\text{Mn-Mn}}^0$  for  $\text{X} = \text{Rh}$  and, on the other hand, the significant increase for  $\text{X} = \text{Cu}$ . The authors of Ref. [9] assumed that the principal role of the X atoms is to simply determine the size of the crystal lattice. To check this assumption, we calculated  $J_0$  for  $\text{Ni}_2\text{MnSn}$  but with a lattice parameter that is characteristic for  $\text{Cu}_2\text{MnSn}$ . As a result,  $J_{\text{X-Mn}}^0 = 1.3 \text{ mRy}$  and  $J_{\text{Mn-Mn}}^0 = 2.3 \text{ mRy}$  differ strongly from the correctly calculated  $J_0$  of real  $\text{Cu}_2\text{MnSn}$  by  $0.3 \text{ mRy}$  and  $5.7 \text{ mRy}$  respectively (see Tab. II). Also, the modified exchange parameters upon  $d$ -metal substitution is not reproduced by the RBA which worked nicely for an  $sp$ -component substitution.

In order to analyze the problem in more detail, we show the course of  $J(E)$  as a func-

tion of  $\text{Co}_2\text{MnSn}$  band filling in Fig. 9. The vertical lines correspond to the Fermi levels where the total number of valence electrons is equal to the corresponding compound of the  $\text{X}_2\text{MnSn}$  family. While it is clear that  $J$  continuously decreases upon  $\text{Co} \rightarrow \text{Ni}$  (and also  $\text{Cu}$ ) substitution, this lowering is *underestimated*, and the effective  $J_{\text{Mn}}^0$  obtained from Fig. 9 is close to 8 mRy but the properly calculated  $J_{\text{Mn}}^0$  is 5 mRy (see Tab. II).

The predicted Curie temperatures obtained from the calculated parameters are presented in Tab. I. The correct tendency for the calculated Curie temperatures has been mentioned above, except for  $\text{Ni}_2\text{MnSn}$  where the disagreement is within the accuracy of the method. The total exchange parameter  $J_0$  is mostly determined by the first X–Mn pair interaction and has significant long-range contributions; at least six interactions are important, see Tab. VI. We also include the results obtained from total-energy calculations [9] and from a fit to spin-wave dispersions [16]. The exchange coupling in the LWA produces somewhat smaller values for Mn–Mn interaction while X–Mn interactions are underestimated by 50-60% when compared with those from the general definition (eq. 6). All  $T_C$ 's are overestimated in this approach and we expect that any improvement of the MFA will produce better agreement with experiment. The calculated exchange parameters can be used in any more sophisticated calculations of the critical temperature.

As mentioned before, one can compare the Mn total exchange only. The  $J_{ij}$  obtained in Ref. [9] are in good agreement with our results for  $\text{Pd}_2\text{MnSn}$  (2.1 mRy and 2.5 mRy respectively), but for the Ni- and Cu-based compounds, the authors obtained numbers which are two to three times smaller than ours. The result obtained from spin-wave dispersions in  $\text{Ni}_2\text{MnSn}$  (3.3 mRy) is fairly close to our 4.4 mRy but for  $\text{Pd}_2\text{MnSn}$ , however, the disagreement is significant (1.3 mRy versus 2.5 mRy). Nonetheless, it must be mentioned that both calculations of exchange parameters did *not* include the Mn–X interactions which are important especially in the  $\text{Ni}_2\text{MnSn}$  system. The results obtained from the energy differences of FM and AFM ordered structures tend to give systematically underestimated exchange parameters although these systems are considered as localized-moment systems. The results from spin-wave analysis also underestimate the exchange coupling. We therefore plan to consider the spin-wave properties in future publications.

## V. CONCLUSION

The electronic structures and magnetic exchange interactions have been calculated for a set of full-Heusler alloys with generic formula  $X_2MnZ$  where  $X$  is a transition-metal atom and  $Z$  is an  $sp$  main-group element. The alloy variations of the Curie temperatures calculated in the mean-field approximation are in good agreement with experimental data. Our analysis demonstrates that the  $J_{ij}$  dependence on the  $Z$  atom may be described within a rigid band approximation, having straightforward implications for the influence of the atomic volume of  $Z$ , thereby allowing semi-quantitative predictions. The substitution of an  $X$  element, however, poses a problem for the rigid-band approximation although qualitative tendencies can be identified; for obtaining quantitative results, a full calculation has to be performed. The magnetic exchange parameters and also Curie temperatures decrease along the row  $Cu \rightarrow Ni \rightarrow Rh \rightarrow Pd$ , in agreement with the degree of  $d$  localization for the transition metal. The  $X$ - $Mn$  interactions are very important for systems with sizable magnetic moments on the transition metal ( $Co$ ,  $Rh$  and  $Ni$ ). The  $X$ - $Mn$  interactions are limited by first neighbors while  $Mn$ - $Mn$  interactions are quite long ranged.

This work was carried out, in part, at Ames Laboratory, which is operated for the U.S. Department of Energy by Iowa State University under Contract No. W-7405-82. This work was supported by the Director for Energy Research, Office of Basic Energy Sciences of the U.S. Department of Energy. The support by Deutsche Forschungsgemeinschaft (Grant No. DR 342/7-1) is also gratefully acknowledged.

- 
- [1] R. de Groot, P. van Engen, Phys. Rev. Lett. **50** (1983) 2024.
  - [2] S. Ishida, T. Masaki, S. Fujii, S. Asano, Physica B **245** (1998) 1.
  - [3] M. Julliere, Phys. Lett. A **54** (1975) 225.
  - [4] J. S. Moodera, L. R. Kinder, T. M. Wong, R. Meservey, Phys. Rev. Lett. **74** (1995) 3273.
  - [5] B. Dieny, V. S. Speriosu, S. S. P. Parkin, B. A. Gurney, D. R. Wilhoit, D. Mauri, Phys. Rev. B **43** (1991) 1297.
  - [6] O. Heusler, Ann. Phys. **19** (1934) 155.
  - [7] Y. Ishikawa, Physica B **91** (1977) 130.
  - [8] A. Hamzić, R. Asomoza, I.A. Campbell, J. Phys. F **11** (1981) 1441.

- [9] J. Kübler, A. R. Williams, C. B. Sommers, Phys. Rev. B **28** (1983) 1745.
- [10] I. Galanakis, P. H. Dederichs, N. Papanikolaus, Phys. Rev. B **66** (2002) 174429.
- [11] S. Picozzi, A. Continenza, A. J. Freeman, Phys. Rev. B **66** (2002) 094421.
- [12] A. Ayuela, J. Enkovaara, K. Ullakko, R. M. Nieminen, J. Phys.: Condens. Matter **11** (1999) 2017.
- [13] S. Fujii, S. Ishida, S. Asano, J. Phys. Soc. Jpn **64** (1995) 185.
- [14] S. Ishida, S. Fujii, S. Kashiwagi, S. Asano, J. Phys. Soc. Jpn. **64** (1995) 2152.
- [15] S. Fujii, S. Sugimura, S. Ishida, S. Asano, J. Phys.: Condens. Matter **2** (1990) 8583.
- [16] Y. Noda, Y. Ishikawa, J. Phys. Soc. Jpn. **40** (1976) 690.
- [17] P. J. Webster, Contemp. Phys. **10** (1969) 559.
- [18] Y. Kurtulus, R. Dronskowski, J. Solid State Chem. **176** (2003) 390.
- [19] O. K. Andersen, Phys. Rev. B **12** (1975) 3060.
- [20] O. K. Andersen, O. Jepsen, Phys. Rev. Lett. **53** (1984) 2571.
- [21] S. H. Vosko, L. Wilk, M. Nusair, Can. J. Phys. **58**, (1980) 1200.
- [22] V. P. Antropov, J. Magn. Magn. Mat. **262** (2003) L193.
- [23] A. L. Lichtenstein, M. I. Katsnelson, V. A. Gubanov, J.Phys.F **14** (1984) L125.
- [24] V. P. Antropov, B. N. Harmon, A. N. Smirnov, J. Magn. Magn. Mat. **200**, (1999) 148.
- [25] Here we stick to the physics jargon in that “hybridization” means what chemists would call “orbital interaction”, not to be confused with a unitary transformation into another set of non-orthogonal but localized orbitals.
- [26] G. A. Landrum, R. Dronskowski, Angew. Chem. Int. Ed. **39** (2000) 1560.
- [27] R. Dronskowski, Adv. Solid State Phys. **42** (2002) 433.
- [28] M. van Schilfgaarde, V. P. Antropov, J. Appl. Phys. **85** (1999) 4827.
- [29] V. P. Antropov, M. I. Katshelson, A. I. Liechtenstein, Physica B **237–238** (1997) 336.
- [30] H. Masumoto, K. Watanabe, J. Phys. Soc. Jpn. **32** (1972) 281.
- [31] P. J. Webster, K. R. A. Ziebeck, in *Alloys and Compounds of d-Elements with Main Group Elements*, Part 2, Edited by H. R. J. Wijn, Landolt-Börnstein, New Series, Group III, Vol. 19/c (Springer, Berlin, 1988), pp. 75–184.



TABLE I: Experimental lattice parameters  $a$ , calculated partial and experimental total magnetic moments  $\mu$ , and calculated and experimental Curie temperatures  $T_C$  for  $X_2MnZ$  compounds. All experimental values have been taken from Ref. [31]

compound	$a$ (a.u.)	$\mu_{\text{calc}} (\mu_B)$			$\mu_{\text{expt}} (\mu_B)$		$T_C$ (K)		
		X	Mn	total	total	LWA	exact	expt	
$\text{Co}_2\text{MnGa}$	10.904	0.73	2.78	4.13	4.05	635	880	694	
$\text{Co}_2\text{MnSi}$	10.685	1.01	3.08	5.00	5.07	1251	1563	985	
$\text{Co}_2\text{MnGe}$	10.853	0.97	3.14	5.00	5.11	1115	1417	905	
$\text{Co}_2\text{MnSn}$	11.338	0.95	3.24	5.04	5.08	1063	1325	829	
$\text{Rh}_2\text{MnGe}$	11.325	0.42	3.67	4.49	4.62	410	549	450	
$\text{Rh}_2\text{MnSn}$	11.815	0.45	3.73	4.60	3.10	435	585	412	
$\text{Rh}_2\text{MnPb}$	11.966	0.45	3.69	4.58	4.12	423	579	338	
$\text{Ni}_2\text{MnSn}$	11.439	0.23	3.57	3.97	4.05	373	503	344	
$\text{Cu}_2\text{MnSn}$	11.665	0.04	3.79	3.81	4.11	602	680	530	
$\text{Pd}_2\text{MnSn}$	12.056	0.07	4.02	4.07	4.23	232	275	189	

TABLE II: Sublattices contributions  $J_{nm}^0$  (in mRy) to the effective magnetic exchange parameters  $J_n^0 = \sum_m J_{nm}^0$  for the  $X_2MnZ$  group of compounds (both long wave approximation and exact adiabatic results are shown).

compound	X-X		X-Mn		Mn-Mn	
	$J^{lw}$	$J$	$J^{lw}$	$J$	$J^{lw}$	$J$
Co <sub>2</sub> MnGa	-0.36	-0.21	5.8	7.31	0.81	0.89
Co <sub>2</sub> MnSi	1.57	2.6	10.2	11.4	1.83	1.85
Co <sub>2</sub> MnGe	1.12	2.3	8.92	10.1	2.20	2.2
Co <sub>2</sub> MnSn	0.55	0.94	8.66	9.9	2.24	2.3
Rh <sub>2</sub> MnGe	0.06	0.2	3.17	4.0	1.28	1.31
Rh <sub>2</sub> MnSn	0.11	0.25	3.38	4.25	1.29	1.38
Rh <sub>2</sub> MnPb	0.14	0.38	3.24	4.15	1.32	1.35
Ni <sub>2</sub> MnSn	-0.064	-0.1	1.92	2.8	2.52	2.63
Cu <sub>2</sub> MnSn	0.00	0.01	0.26	0.40	5.71	5.9
Pd <sub>2</sub> MnSn	0.00	0.01	0.29	0.41	2.17	2.34

TABLE III: Pair exchange interaction parameters  $J_{ij}$  (in  $\mu\text{Ry}$ ) in the long-wave approximation for the  $\text{Co}_2\text{MnZ}$  ( $Z = \text{Ga}, \text{Si}, \text{Ge}$  or  $\text{Sn}$ ) family and results from Ref. [9].

compound	sublatt.	$J_1$	$J_2$	$J_3$	$J_4$	$J_5$	$J_6$	$J_7$	$J_8$
$\text{Co}_2\text{MnGa}$	$\text{Co}_1\text{-Co}_1$	-11	4	-7	-7	2	2	1	1
	$\text{Co}_1\text{-Co}_2$	49	4	-76	-5	0	-3	2	1
	$\text{Co}_1\text{-Mn}$	557	64	-5	-3	-1	-3	0	0
	$\text{Mn-Mn}$	36	-2	4	17	2	-3	8	3
$\text{Co}_2\text{MnSi}$	$\text{Co}_1\text{-Co}_1$	5	59	1	1	1	-2	1	1
	$\text{Co}_1\text{-Co}_2$	165	72	-31	-6	10	0	2	1
	$\text{Co}_1\text{-Mn}$	1106	38	12	2	4	1	0	0
	$\text{Mn-Mn}$	130	58	-12	24	0	-8	0	-2
$\text{Co}_2\text{MnGe}$	$\text{Co}_1\text{-Co}_1$	-11	55	2	2	1	-2	0	0
	$\text{Co}_1\text{-Co}_2$	136	75	-53	-5	10	-1	2	1
	$\text{Co}_1\text{-Mn}$	932	41	11	3	6	1	0	0
	$\text{Mn-Mn}$	141	60	-5	23	1	-5	1	-4
$\text{Co}_2\text{MnSn}$	$\text{Co}_1\text{-Co}_1$	-40	57	4	4	2	-5	0	0
	$\text{Co}_1\text{-Co}_2$	73	87	-56	-6	13	-4	2	4
	$\text{Co}_1\text{-Mn}$	907	40	7	0	9	2	4	1
	$\text{Co}_1\text{-Mn}$	907	40	7	0	9	2	4	1
	$\text{Mn-Mn}$	126	78	5	26	-3	-13	0	0
	$\text{Mn-Mn}^{[9]}$	630	135						

TABLE IV: The radius-vector  $\mathbf{r}$ , the distance from the central atom  $r$ , and the number of equivalent nearest neighbors  $n$  for the L2<sub>1</sub> type of structures.

$J_i$	X <sub>1</sub> -X <sub>1</sub>			X <sub>1</sub> -X <sub>2</sub>			X <sub>1</sub> -Mn			Mn-Mn		
	$n$	$r$	$\mathbf{r}$	$n$	$r$	$\mathbf{r}$	$n$	$r$	$\mathbf{r}$	$n$	$r$	$\mathbf{r}$
$J_1$	12	0.707	$\frac{\bar{1}\bar{1}}{2}0$	6	0.500	$0\frac{1}{2}0$	4	0.433	$\frac{1}{4}\frac{1}{4}\frac{1}{4}$	12	0.707	$\frac{\bar{1}\bar{1}}{2}0$
$J_2$	6	1.000	$00\bar{1}$	4	0.866	$\frac{\bar{1}\bar{1}}{2}\frac{\bar{1}}{2}$	12	0.829	$\frac{\bar{1}}{4}\frac{3}{4}\frac{1}{4}$	6	1.000	$00\bar{1}$
$J_3$	12	1.225	$\frac{\bar{1}\bar{1}}{2}\frac{\bar{1}}{2}$	4	0.866	$\frac{\bar{1}\bar{1}}{2}\frac{1}{2}$	12	1.090	$\frac{3}{4}\frac{1}{4}\frac{3}{4}$	24	1.225	$\frac{\bar{1}\bar{1}}{2}\frac{\bar{1}}{2}$
$J_4$	12	1.225	$1\frac{\bar{1}\bar{1}}{2}$	24	1.118	$\frac{\bar{1}}{2}0\bar{1}$	12	1.299	$\frac{5}{4}\frac{\bar{1}}{4}\frac{1}{4}$	12	1.414	$\bar{1}\bar{1}0$
$J_5$	12	1.414	$\bar{1}\bar{1}0$	6	1.500	$00\frac{\bar{3}}{2}$	4	1.299	$\frac{\bar{3}}{4}\frac{3}{4}\frac{3}{4}$	24	1.581	$0\frac{\bar{1}\bar{3}}{2}$
$J_6$	24	1.581	$0\frac{\bar{1}\bar{3}}{2}$	12	1.500	$\bar{1}\frac{\bar{1}}{2}\bar{1}$	24	1.479	$\frac{5}{4}\frac{3}{4}\frac{\bar{1}}{4}$	8	1.732	$\bar{1}\bar{1}\bar{1}$
$J_7$	4	1.732	$\bar{1}\bar{1}\bar{1}$	12	1.500	$\bar{1}\frac{1}{2}\bar{1}$	12	1.639	$\frac{3}{4}\frac{5}{4}\frac{3}{4}$	48	1.871	$\frac{3}{2}1\frac{1}{2}$
$J_8$	4	1.732	$\bar{1}\bar{1}\bar{1}$	12	1.658	$\frac{1}{2}\frac{\bar{3}}{2}\frac{1}{2}$	12	1.785	$\frac{1}{4}\frac{7}{4}\frac{1}{4}$	6	2.000	$00\bar{2}$

TABLE V: Pair magnetic exchange interactions  $J_{ij}$  (in  $\mu\text{Ry}$ ) in the long-wave approximation calculated for  $\text{Rh}_2\text{MnZ}$  ( $Z = \text{Ge}, \text{Sn}$  or  $\text{Pb}$ ).

compound	sublatt.	$J_1$	$J_2$	$J_3$	$J_4$	$J_5$	$J_6$	$J_7$	$J_8$
$\text{Rh}_2\text{MnGe}$	$\text{Rh}_1\text{-Rh}_1$	-9	13	0	0	-1	0	0	0
	$\text{Rh}_1\text{-Rh}_2$	17	0	-3	-2	6	0	0	1
	$\text{Rh}_1\text{-Mn}$	312	21	2	2	2	1	0	-1
	$\text{Mn-Mn}$	87	102	3	18	-5	-27	-4	-9
$\text{Rh}_2\text{MnSn}$	$\text{Rh}_1\text{-Rh}_1$	-8	15	0	0	-2	0	0	0
	$\text{Rh}_1\text{-Rh}_2$	20	2	-3	-2	8	-1	0	1
	$\text{Rh}_1\text{-Mn}$	340	20	3	2	2	1	1	-1
	$\text{Mn-Mn}$	61	108	6	29	-6	-27	-4	-3
$\text{Rh}_2\text{MnPb}$	$\text{Rh}_1\text{-Rh}_1$	-8	15	0	0	-2	1	-1	-1
	$\text{Rh}_1\text{-Rh}_2$	22	2	-5	-2	7	-1	0	1
	$\text{Rh}_1\text{-Mn}$	327	17	5	2	1	1	1	-1
	$\text{Mn-Mn}$	57	96	21	33	-8	-34	-9	-4

TABLE VI: Pair magnetic exchange interactions  $J_{ij}$  (in  $\mu\text{Ry}$ ) in the long-wave approximation calculated for  $\text{X}_2\text{MnSn}$  ( $\text{X} = \text{Ni}, \text{Cu}$  or  $\text{Pd}$ ) and results from Refs. [9, 16].

compound	sublatt.	$J_1$	$J_2$	$J_3$	$J_4$	$J_5$	$J_6$	$J_7$	$J_8$
$\text{Ni}_2\text{MnSn}$	$\text{Ni}_1\text{-Mn}$	263	-18	1	4	8	1	1	2
	$\text{Mn-Mn}$	151	116	29	-104	14	-30	12	-14
	$\text{Mn-Mn}^{[9]}$	187	-13						
	$\text{Mn-Mn}^{[16]}$	82	105	38	37	-6	17	4	2
$\text{Cu}_2\text{MnSn}$	$\text{Cu}_1\text{-Mn}$	30	2	0	0	-1	0	0	0
	$\text{Mn-Mn}$	491	318	-118	19	-12	65	9	9
	$\text{Mn-Mn}^{[9]}$	88	97						
$\text{Pd}_2\text{MnPb}$	$\text{Pd}_1\text{-Mn}$	40	-3	0	0	2	0	0	0
	$\text{Mn-Mn}$	65	116	51	-78	20	-64	16	-5
	$\text{Mn-Mn}^{[9]}$	187	-20						
	$\text{Mn-Mn}^{[16]}$	64	43	21	-44	14	-19	4	-6

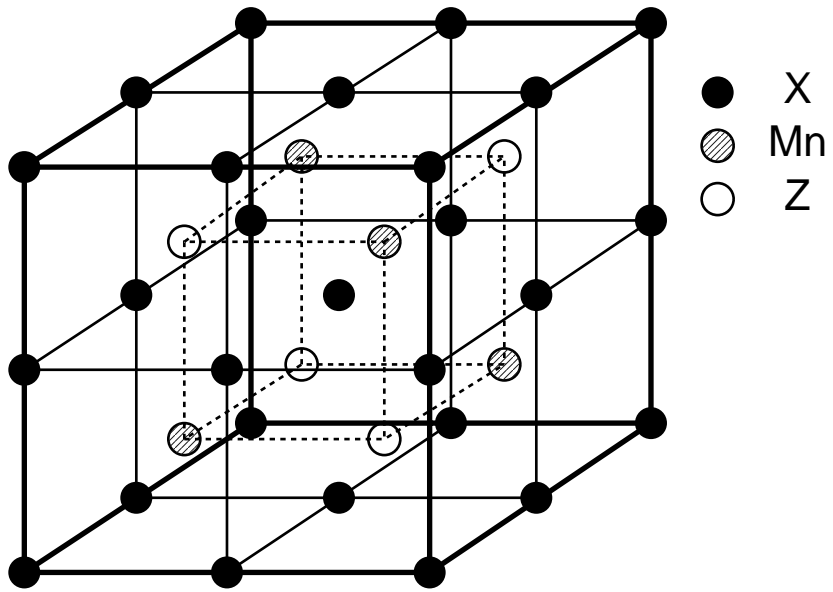


FIG. 1: The L<sub>21</sub> structure type composed of four interpenetrating fcc lattices.

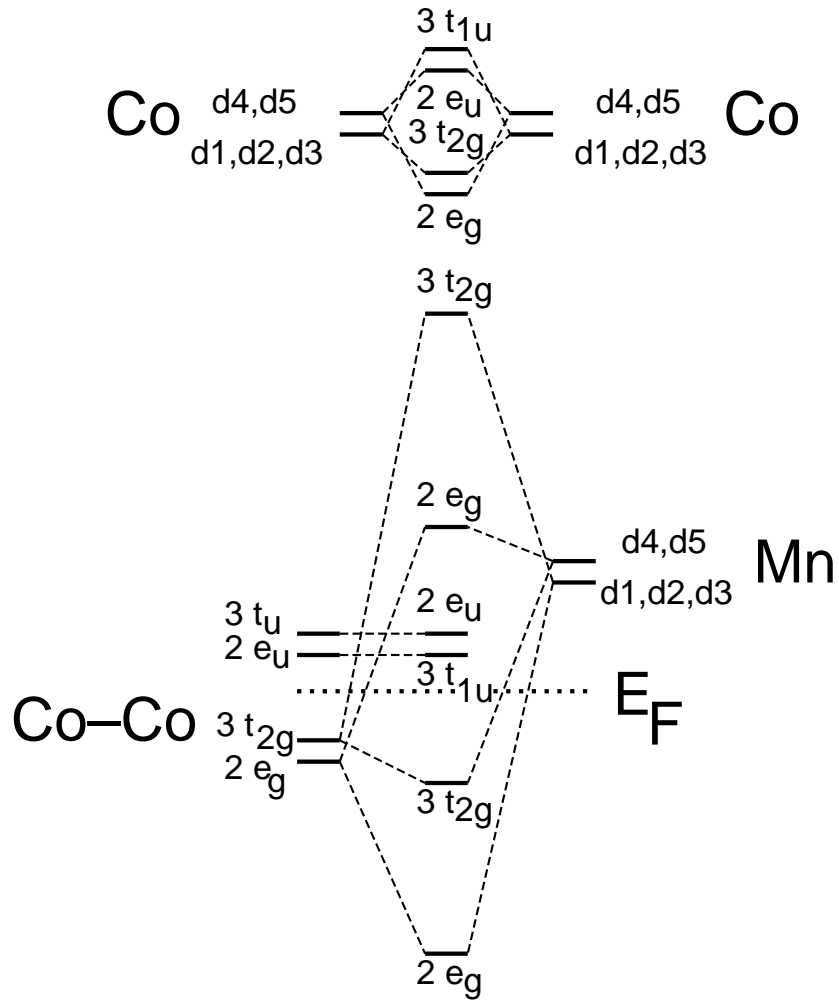


FIG. 2: Schematic hybridization between the minority spin orbitals of  $\text{Co}_2\text{MnGa}$ , first between two Co atoms (top), then between two Co atoms and a neighboring Mn atom (bottom). The coefficients label the degeneracies of the orbital sets (see notations in Ref. [10])



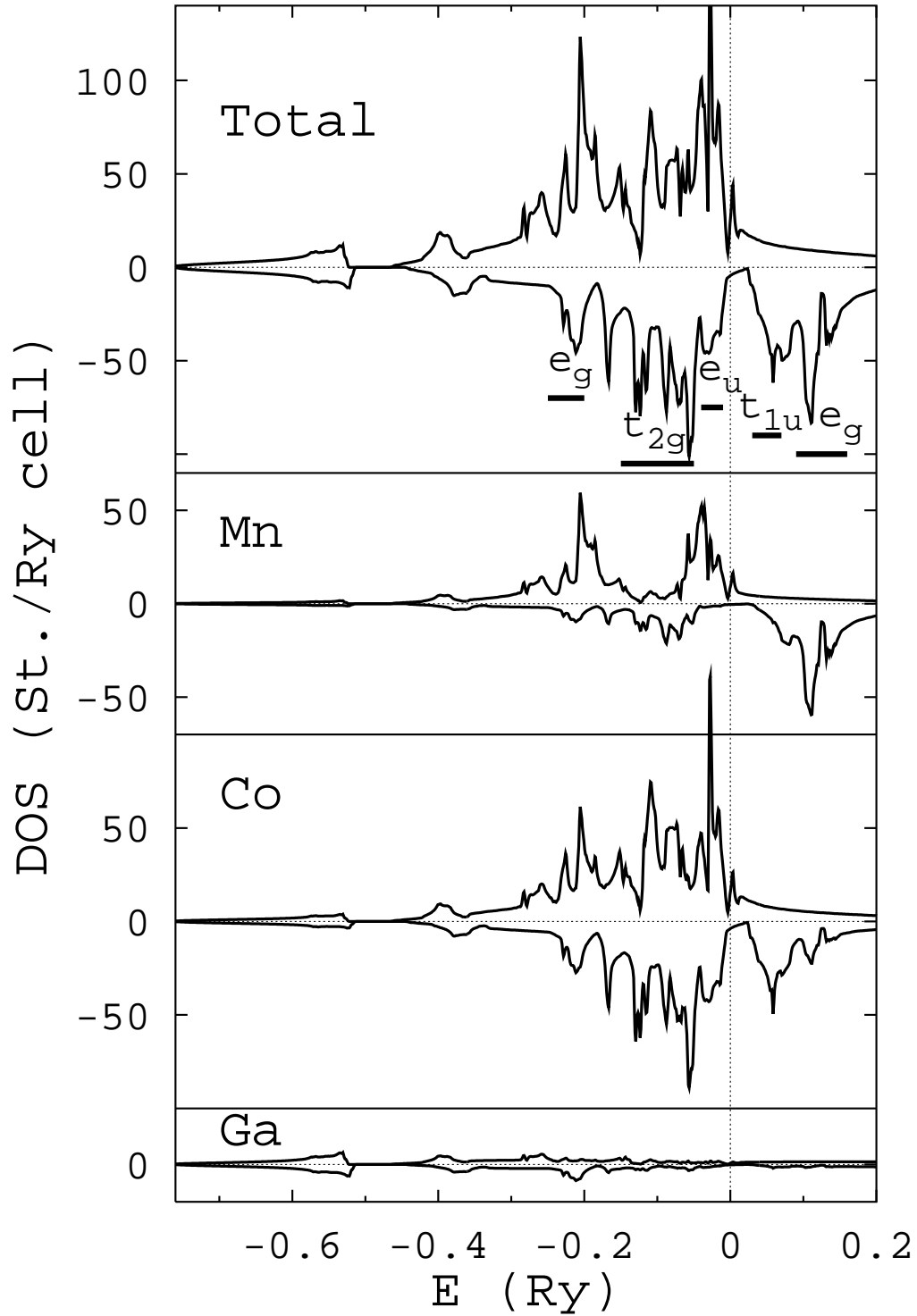


FIG. 3: Total and partial DOS for the compound  $\text{Co}_2\text{MnGa}$ . The character of each peak belonging to the minority spin states has been indicated, and the Fermi level is set to the energy zero.

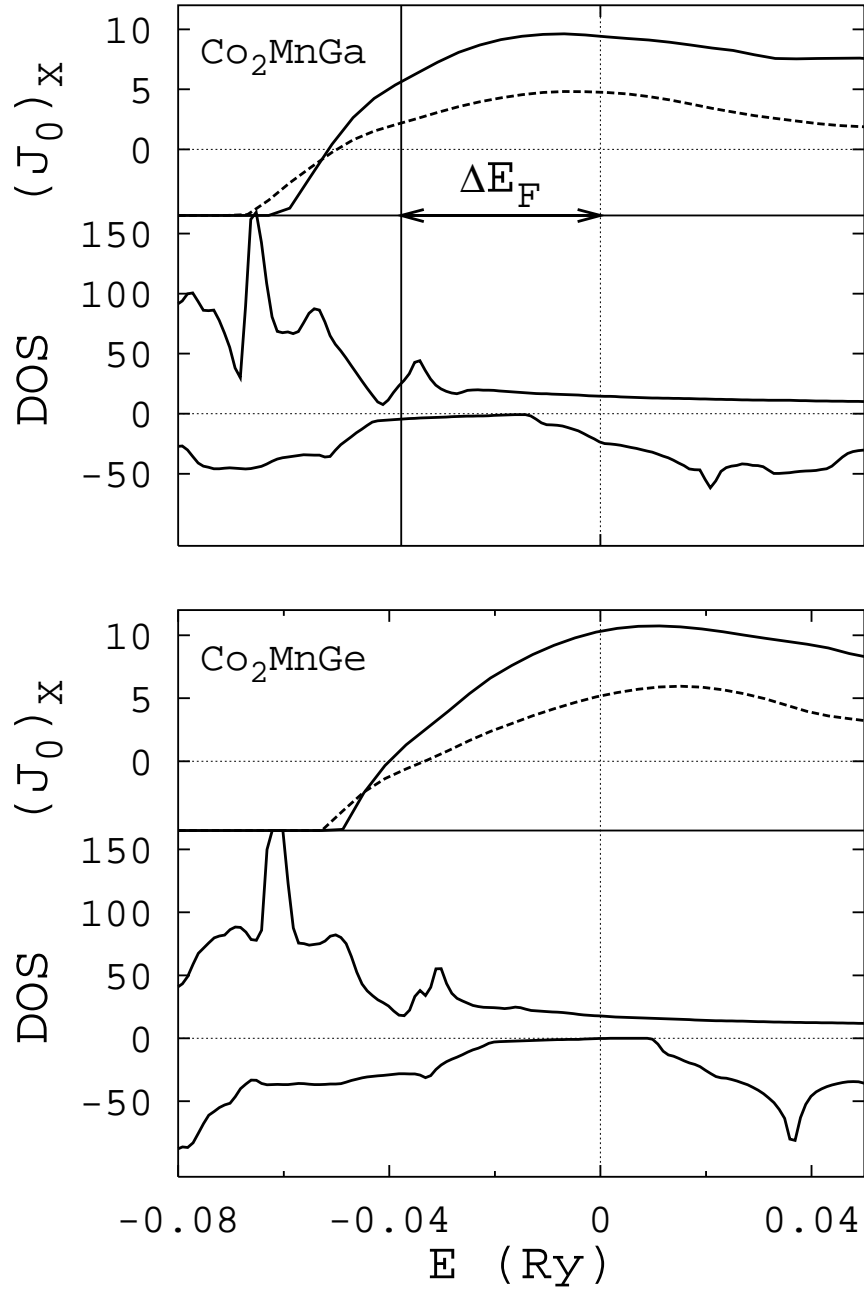


FIG. 4: Density of states and  $J^0(E)$  for the Mn (solid line) and Co (dashed line) atoms of  $\text{Co}_2\text{MnGa}$  (top) and  $\text{Co}_2\text{MnGe}$  (bottom). The Fermi level is at zero energy for  $\text{Co}_2\text{MnGe}$  (29 valence electrons) and shifted to the left for  $\text{Co}_2\text{MnGa}$  (28 valence electrons) by the rigid-band shift  $\Delta E_F$ .

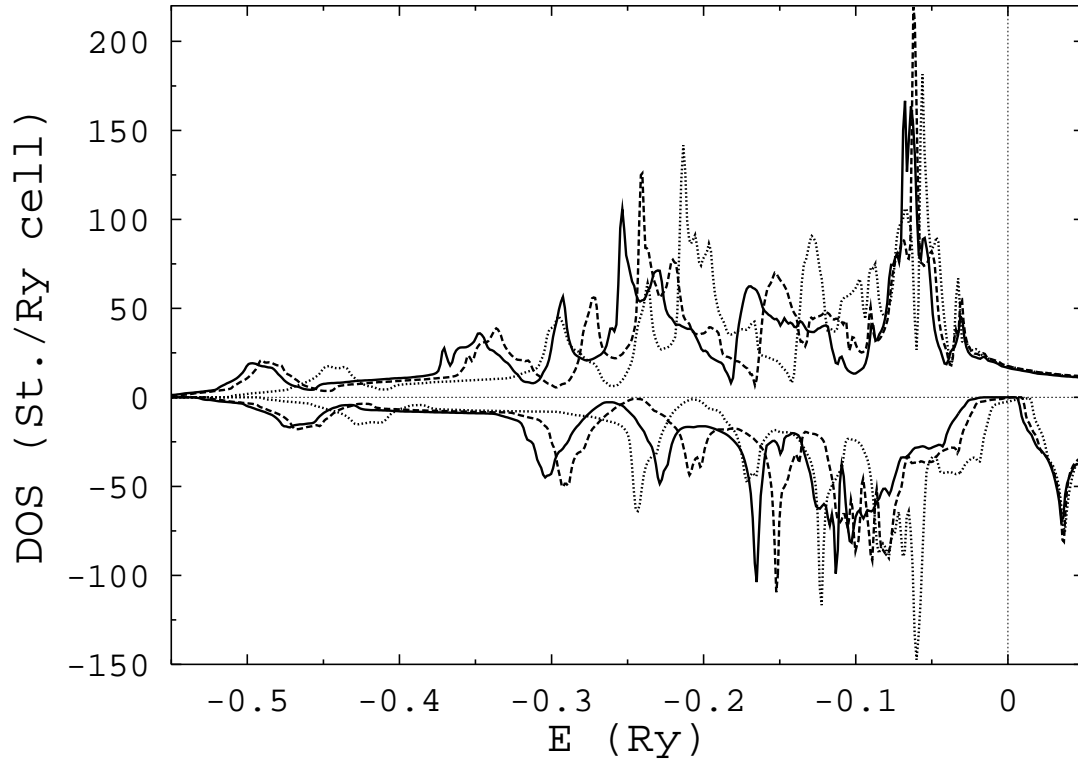


FIG. 5: Density of states of the compounds Co<sub>2</sub>MnSi (solid line), Co<sub>2</sub>MnGe (dashed line) and Co<sub>2</sub>MnSn (dotted line). The Fermi level is at the energy zero.

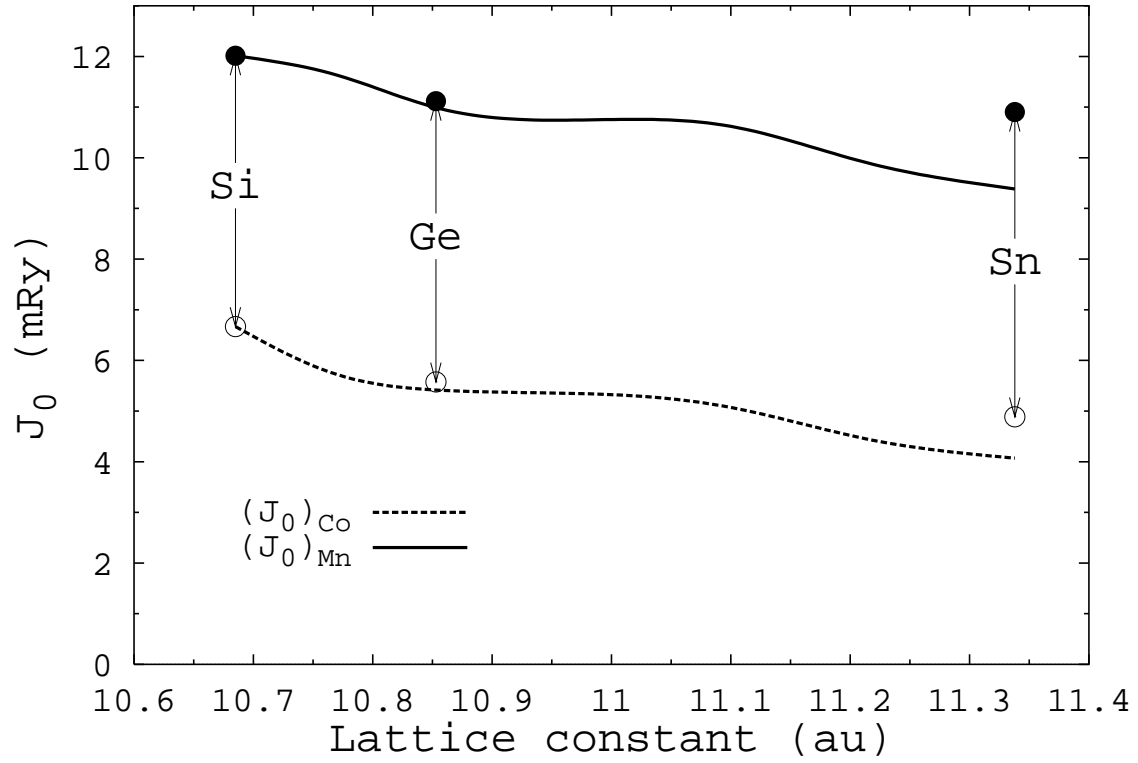


FIG. 6: Course of  $J_{\text{Mn}}^0$  (solid line) and  $J_{\text{Co}}^0$  (dashed line) as a function of the lattice parameter in  $\text{Co}_2\text{MnSi}$ . Filled circles correspond to  $J_{\text{Mn}}^0$  and empty ones to  $J_{\text{Co}}^0$  for  $\text{Co}_2\text{MnZ}$  systems ( $Z = \text{Si}$ ,  $\text{Ge}$  and  $\text{Sn}$ ) calculated at their experimental lattice parameters.

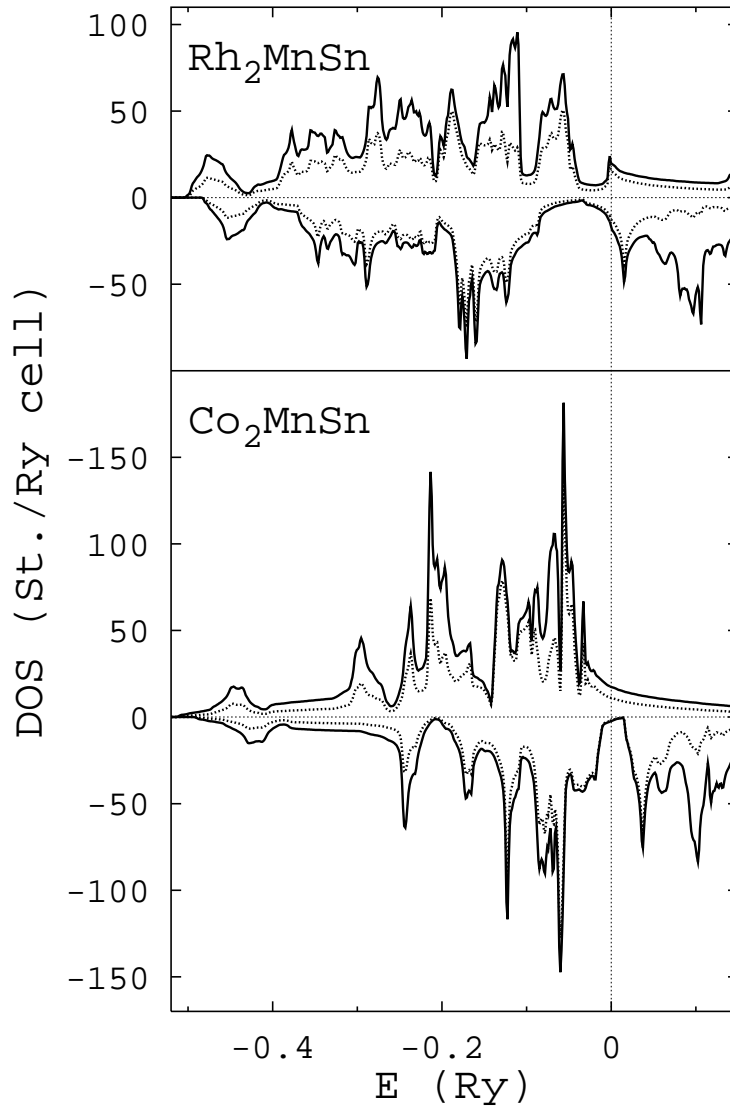


FIG. 7: Total (solid line) and partial densities of states (dashed line) of Mn in  $\text{Rh}_2\text{MnSn}$  and  $\text{Co}_2\text{MnSn}$ . The Fermi level is at the energy zero.

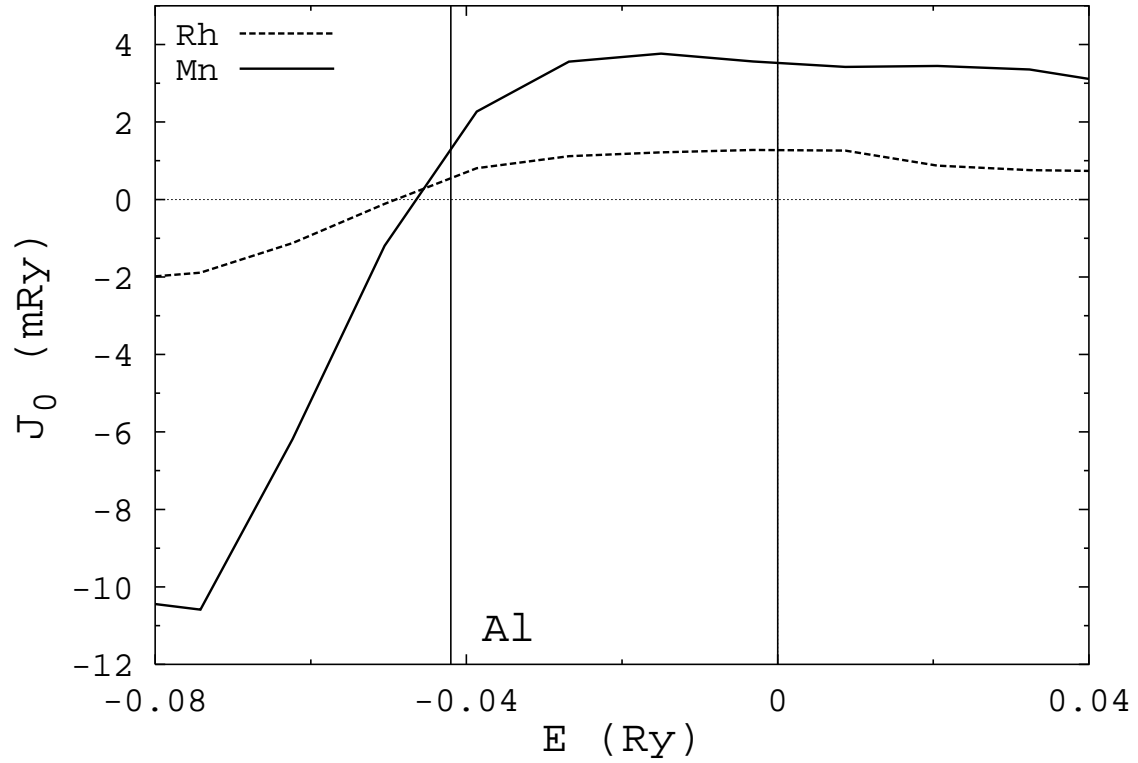


FIG. 8: The calculated effective exchange parameters  $J_{\text{Mn}}^0$  (solid) and  $J_{\text{Rh}}^0$  (dashed line) as a function of band filling for  $\text{Rh}_2\text{MnGe}$ . Vertical lines corresponds to 28 ( $\text{Rh}_2\text{MnAl}$ ) and 29 ( $\text{Rh}_2\text{MnGe}$ ) electrons per unit cell. The energy zero corresponds to the Fermi level of  $\text{Rh}_2\text{MnGe}$ .

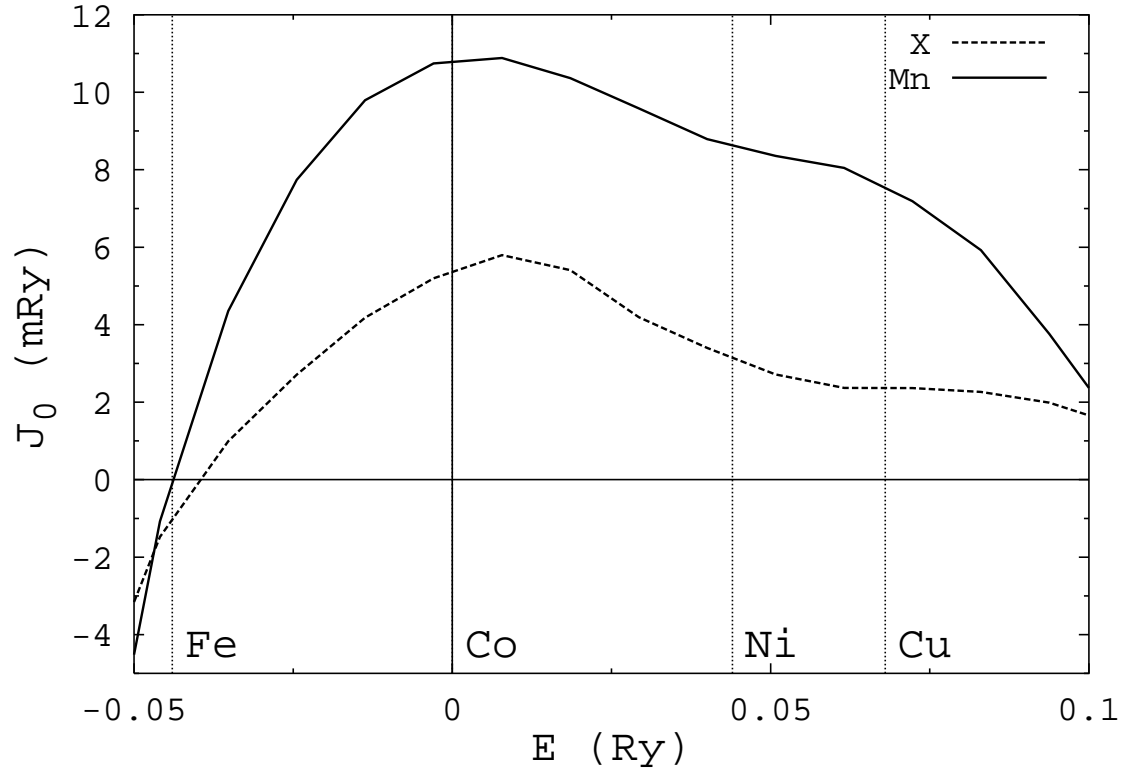


FIG. 9: The calculated effective parameters  $J_{\text{Mn}}^0$  (solid line) and  $J_{\text{Co}}^0$  (dashed line) as a function of band filling in  $\text{Co}_2\text{MnSn}$ . Vertical lines correspond to 27 ( $\text{Fe}_2\text{MnSn}$ ), 29 ( $\text{Co}_2\text{MnSn}$ ), 31 ( $\text{Ni}_2\text{MnSn}$ ) and 33 ( $\text{Cu}_2\text{MnSn}$ ) electrons per unit cell.